Food Chemistry 339 (2021) 127854

Contents lists available at ScienceDirect

Food Chemistry

journal homepage: www.elsevier.com/locate/foodchem

Metal-polydopamine framework based lateral flow assay for high sensitive detection of tetracycline in food samples

Yongming Tian[1], Tong Bu[1], Meng Zhang, Xinyu Sun, Pei Jia, Qinzhi Wang, Yingnan Liu, Feier Bai, Shuang Zhao, Li Wang*

College of Food Science and Engineering, Northwest A&F University, Yangling 712100, Shannxi, China

ARTICLE INFO

Keywords:
Lateral flow assay
Metal-polydopamine framework
Tetracycline
Food analysis

ABSTRACT

Gold nanoparticles (AuNPs)-based lateral flow assay (LFA) enables a rapid detection of tetracycline (TET) in food samples but suffers from low sensitivity. Herein, metal-polydopamine framework (MPF), as a label, was employed to load monoclonal antibodies (mAbs) directly as the probe in LFA for highly sensitive sensing of TET. Combining zeolitic imidazolate framework (ZIF-67) and polydopamine (PDA), a stable MPF with large size, well water-dispersible, excellent affinity and optical properties was prepared through a versatile layer-by-layer assembly (LLA) strategy. Under optimized conditions, the biosensor (MPF-LFA) exhibited a great linear relationship in the range of 0.09–6 ng/mL and a detection limit of 0.045 ng/mL for TET detection, which was over 66-fold more sensitive than traditional AuNPs based LFA. Furthermore, the MPF-LFA was successfully applied to the screening of TET in fish, chicken, milk and shrimp samples with satisfied recoveries from 91% to 114%.

1. Introduction

Tetracycline (TET), a broad-spectrum antibiotic, was widely used in combination with many veterinary drugs or feed additives to promote animal growth (El Alami El Hassani et al., 2019; Li et al., 2019; Wang et al., 2020, 2019; Zhang & Chen, 2016). However, the misuse of this drug has inevitably led to its accumulation in animal products, which will increase certain serious risks to human health such as multi-drug resistance of microorganisms, ear injury, and chronic toxicity (Ge et al., 2018; Wang et al., 2018; Yan et al., 2018). To ensure food safety, European Union (EU) has set the maximum residue limits (MRLs) for TET as 100 μg/kg in milk and muscle tissues (Ge et al., 2018; Li, et al., 2017). Thus, it is essential to construct a rapid, sensitive, and facile approach for monitoring TET in animal food products.

Lateral flow assay (LFA) is a promising tool for the identification of analytes owing to its advantages of rapid, simple, cost-effective, real-time approach and user-friendly operation (Bu et al., 2019; Chapman et al., 2015; Gomez-Martinez et al., 2018; Hu et al., 2017; Kim et al., 2018). Unfortunately, the low sensitivity of the traditional gold nanoparticles (AuNPs) based LFA restricts its wide applicability, especially in trace analysis (Chen et al., 2016). In recent years, several alternative labels, such as quantum dots (QDs) (Taranova, Berlina, Zherdev, & Dzantiev, 2015), upconversion NPs (Zhao et al., 2014), and Fe_3O_4 nanospheres (Bragina et al., 2019) can achieve satisfactory sensitivity as labels in LFA sensors. However, they suffer from complicated binding with monoclonal antibodies (mAbs) (typically require an organic cross-linking agent such as ethyl carbodiimide hydrochloride and *N*-hydroxysuccinimide (EDC/NHS) or glutaraldehyde to activate binding), which will result in reducing the activity of the mAbs, thereby affecting the sensitivity. Therefore, an ideal LFA-based detection platform should be based on an “ideal carrier” with a simple preparation process, and outstanding naked-eye LFA signal to achieve high sensitivity. Particularly, metal-organic frameworks (MOFs) are assembled from metal ion clusters and organic ligands (Chen et al., 2018; Dai et al., 2018; Liang et al., 2017; Qiu et al., 2020), which have been applied in gas storage and separation (Qiu, Sharif et al., 2019; Qiu, Ying et al., 2019; Sumida et al., 2012), chemical sensors (Kreno et al., 2011; Qiu, Sharif et al., 2019; Qiu, Ying et al., 2019), biomedicine, and optics (Qin, Wang, & Wang, 2017). Zeolitic imidazolate framework (ZIF-67) as one kind of MOF materials, has a high specific surface area, porous structure, controllable size, and specific optical property (Chen, Yang, Zhu, & Xia, 2014; Mehta et al., 2019; Xu et al., 2019). These features make it a suitable amplifying label for LFA. However, MOF based LFA has not been reported due to the high challenge to construct a MOF based LFA carrier with robust signal.

Herein, in order to improve the sensitivity of detecting TET, a novel

* Corresponding author.
E-mail address: lwang@nwsuaf.edu.cn (L. Wang).
[1] These authors contributed equally to this work.

https://doi.org/10.1016/j.foodchem.2020.127854
Received 13 January 2020; Received in revised form 29 July 2020; Accepted 14 August 2020
Available online 18 August 2020

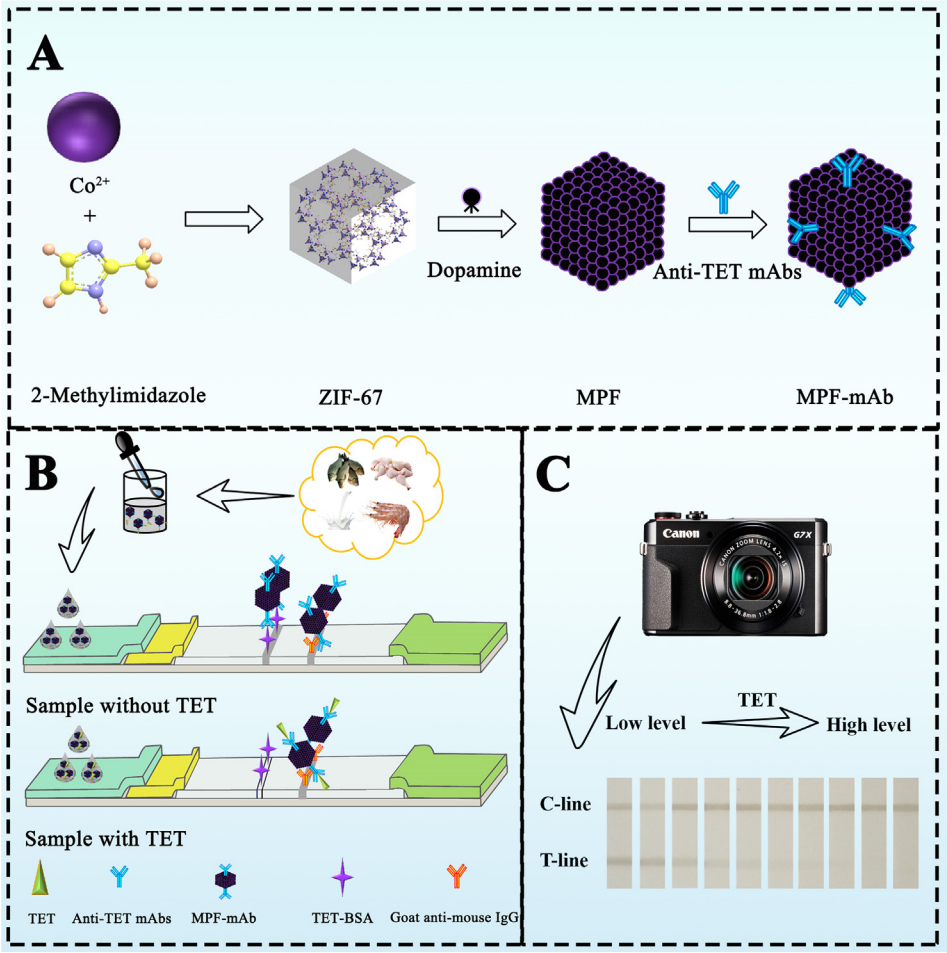

Fig. 1. Schematic illustration of (A) the synthesis procedures of ZIF-67, MPF, and MPF-mAb, (B) the detection of TET by MPF-LFA sensor, (C) the interpretation of the assay results.

metal-polydopamine framework (MPF) based LFA for TET immunoassay was developed. By using ZIF-67 as a precursor, polydopamine (PDA) was then grown on its surface through layer-by-layer assembly (LLA) strategy to form a water-dispersible MPF, which was then applied in LFA system to load mAbs directly. The MPF possessed forceful black color, excellent stability and affinity with mAbs. Moreover, the MPF was labeled by anti-TET mAbs via a simple mixing method without complex cross-linkers, avoiding the drawbacks of the previous carriers. Meanwhile, the MPF could label fewer mAbs than traditional AuNPs, thereby improving the sensitivity. Combining these merits, the MPF-LFA showed a detection limit down to 0.045 ng/mL for TET detection, which was over 66-fold more sensitive than conventional AuNPs-LFA. Besides, the MPF-LFA was successfully applied to detect TET in milk, fish, shrimp, and chicken samples, revealing its application potential in food samples.

2. Material and methods

2.1. Preparation of MPF

ZIF-67 nanocubes were prepared according to previous work with some modifications (Hu, Guan, & Lou, 2016; Ren, Cai, Yu, Zeng, & Tang, 2018). Firstly, 7.264 g 2-methylimidazole was dispersed in 112 mL deionized water under vigorous stirring. Then, Co^{2+} (464 mg) was dissolved in 16 mL 0.1% cetrimonium bromide (CTAB) solution and was immediately added to the above mixture, followed by continuously stirring for 30 min at ambient temperature. Afterward, the precursor was washed by several cycles of centrifugation with ethanol and deionized water. Finally, the obtained ZIF-67 was dried at 60 °C.

MPF was synthesized according to previous work with minor modifications (Ren et al., 2018). Initially, ZIF-67 (40 mg) was dissolved in a mixture (70 mL) of ethanol/aqueous (3:4, v/v) under ultrasonication for 5 min. Next, PDA (16 mg) was added into the solution under vigorous stirring. Then 10 mM Tris-HCl (50 mL, pH 8.5) buffer solution was added and stirred gently to react for overnight. At last, the sediment was centrifuged and cleaned with ethanol and deionized water until the supernatant was clear. The black precipitate was collected and dried at 60 °C.

2.2. Preparation of the MPF-mAb probe

MPF-mAb probe was prepared according to previous work with some modifications (Zhang, Li, Zhang, & Zhang, 2011). Firstly, 40 μg of anti-TET mAbs (1 mg/mL) solution was added to 5 mL MPF suspension (0.6 mg/mL). Afterward, the mixture was incubated for 30 min at ambient temperature under gentle stirring. To block unreacted sites, 10% bovine serum albumin (BSA) solution was added with a final concentration of 1% and shaking for another 30 min. The complex was incubated at 4 °C for 2 h, followed by centrifugation (10,000 rpm, 15 min) to remove unbound protein. The obtained precipitate was resuspended in 0.5 mL of deionized water for further use. The experiment was repeated three times. The fabrication of the ZIF-67-mAb probe using the same method is depicted in the supporting information.

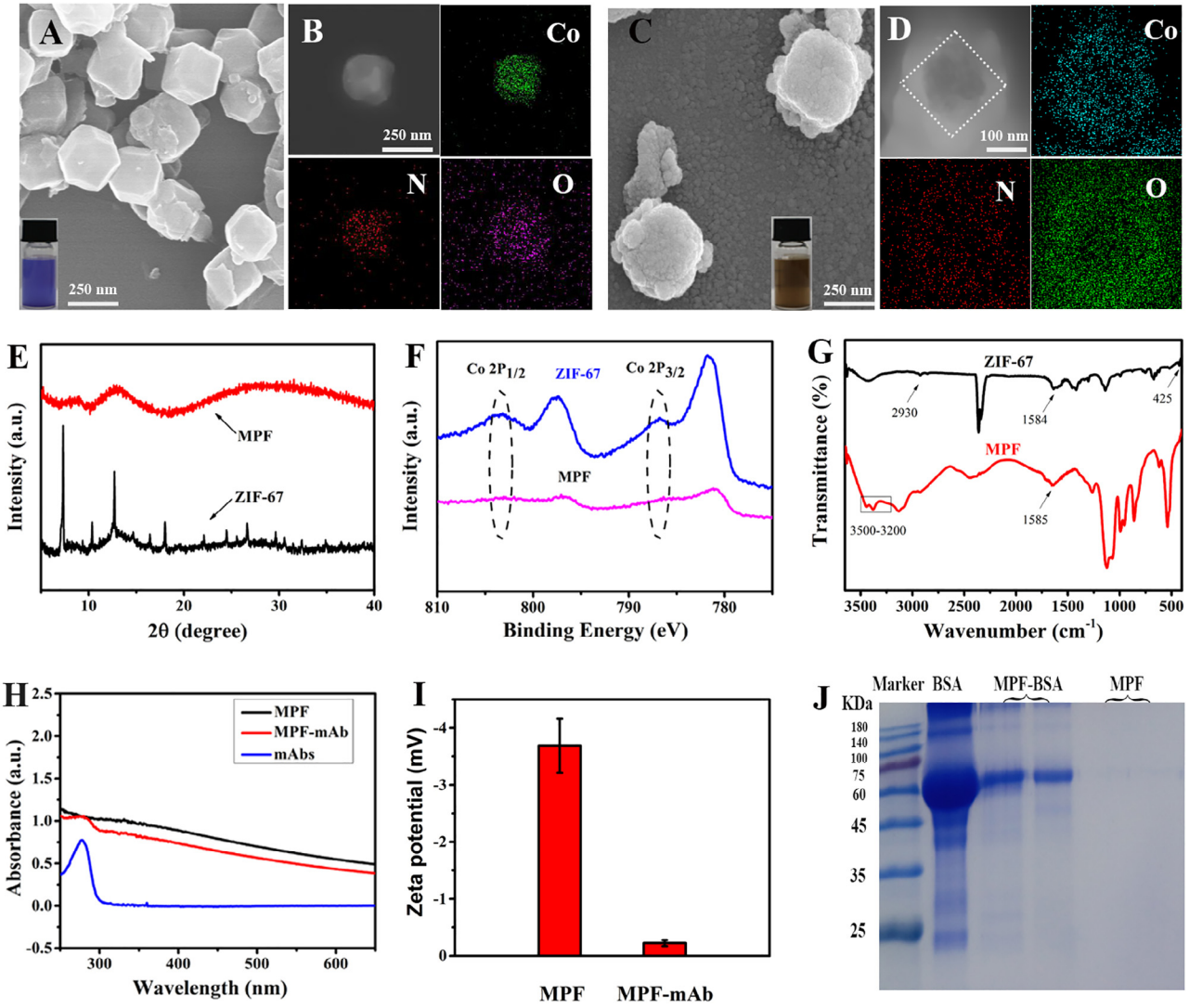

Fig. 2. SEM images and photographs (left inset) of (A) ZIF-67 and (C) MPF, respectively; TEM images and elemental mappings for Co, N, and O of a single particle of (B) ZIF-67 and (D) MPF, respectively; (E)-(G) XRD, XPS, and FT-IR spectra of ZIF-67 and MPF, respectively; (H) UV–vis absorption spectra of mAbs, MPF, and MPF-mAb probe; (I) Zeta potentials of MPF and MPF-mAb; (J) SDS-PAGE images of BSA, MPF- BSA, and MPF, respectively.

2.3. Preparation of the MPF-LFA

The LFA was made up of a sample pad, a conjugate pad, a nitrocellulose (NC) membrane, an absorbent pad, and a plastic scaleboard. By using XYZ dispensing system, TET-BSA (1 mg/mL) and goat anti-mouse immunoglobulin (IgG) (1 mg/mL) were coated on the NC membrane at a dispensing rate of 1 μL/cm to form the test line (*T*-line) and control line (C-line), respectively. Then, the NC membrane was air-dried for 2 h. Subsequently, the sample pad and conjugate pad were blocked by a blocking buffer solution and then stayed in a 37 °C oven for overnight drying. The absorbent pad did not require any treatment. Finally, the sample pad, conjugate pad, NC membrane, and absorbent pad were overlapped 2 mm in turn and attached to the plastic scaleboard, which ensures that probes and TET can migrate through capillary forces throughout the experiment. The composite panel was cut to 3 mm width and then deposited at 4 °C for further use.

2.4. Performance evaluation of MPF-LFA

Firstly, the TET solution was diluted to various concentrations with deionized water (0.023, 0.045, 0.09, 0.18, 0.375, 0.75, 1.5, 3, and 6 ng/mL). Then, 100 μL of each dilution was immediately mixed with 1 μL of MPF-mAb probe, and 100 μL of deionized water was employed as a negative control. After thoroughly mixing with TET, the product was dropped on the sample pad, and it migrated from the sample pad to the test area under capillary force. After reacting for 15 min, the intensities of the C-line and *T*-line were measured by a strip analyzer.

The specificity of the biosensor was determined by testing solutions containing both TET (6 ng/mL) and 11 other antibiotics, namely, oxytetracycline (OXY), chlortetracycline hydrochloride (CTE), amoxicillin (AMX), streptomycin sulphate (STR), florfenicol (FLO), vancomycin hydrochloride (VAN), azithromycin (AZM), kanamycin sulfate (KAN), ampicillin (AMP), neomycin sulfate (NEO), and erythromycin (ERY) (100 ng/mL).

2.5. Sample pretreatment

Food samples were treated according to a previous report (Sheng et al., 2018). For the meat samples, 2 g of the chicken, fish, and shrimp were added to 4 mL of 3% trichloroacetic acid (TA). In addition, 5 mL of milk was mixed with 5 mL of 3% TA. After vortexing for 10 min, the resulting extract was centrifuged at 12,000 rpm for 10 min. The supernatant was then adjusted to neutral with NaOH (1 M), and it was diluted ten folds with deionized water. TET was added to different

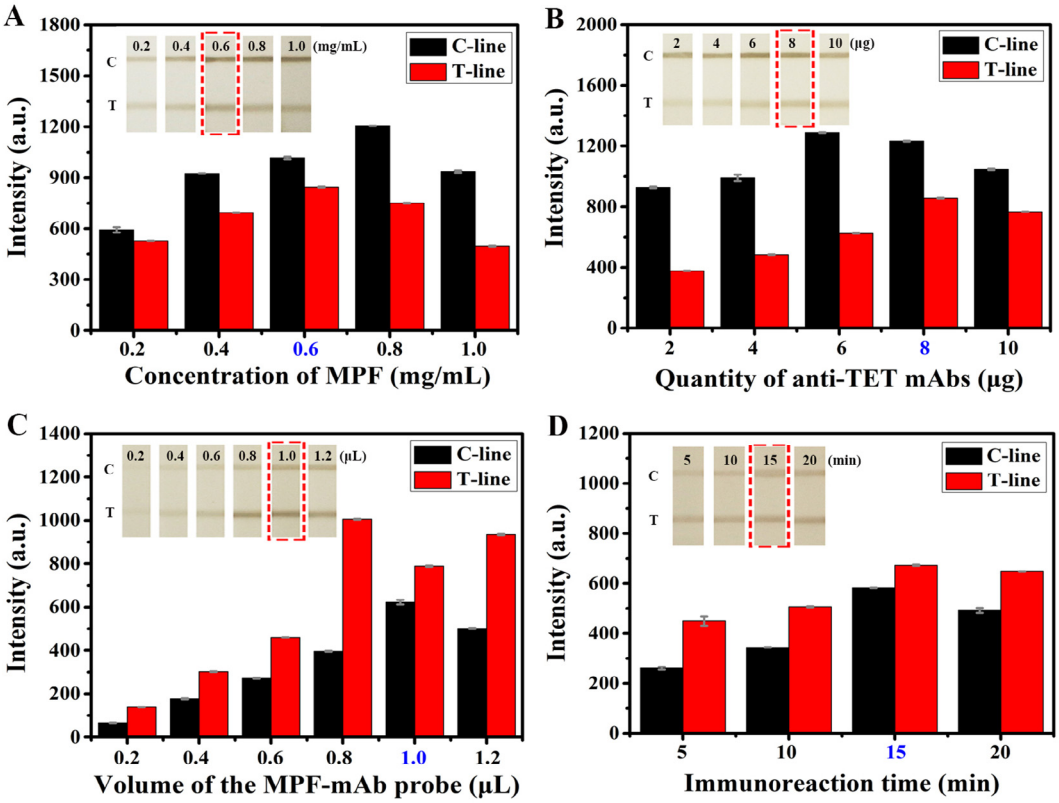

Fig. 3. Effects of (A) the concentration of MPF, (B) the quantity of anti-TET mAbs, (C) the volume of the MPF-mAb probe, and (D) the immunoreaction time on the detection of TET.

sample supernatants and diluted to the different concentrations specified above.

2.6. Statistical analysis

All the tests were performed in triplicate and the data were expressed as mean ± standard deviation (SD). Data analysis was processed through Origin 9.0 software. Difference was considered to be statistically significant if $p < 0.05$.

3. Results and discussion

3.1. Preparation of the MPF and principle of the MPF-LFA biosensor

The synthesis procedures of ZIF-67, MPF, and MPF-mAb were illustrated in Fig. 1A. Firstly, ZIF-67 with exceptional optical property was synthesized. Subsequently, MPF was prepared via covering the surface of ZIF-67 with PDA, making it easier for the material to bond to the mAbs. More importantly, the binding process of MPF to mAbs was straightforward and effortless to operate, just needing simple oscillation and incubation. As demonstrated in Fig. 1B, the MPF-LFA was developed based on the competitive strategy. During the assay, a mixture of the sample and probe was applied to the sample pad, and the complex immediately migrated to the test zone by capillary force. In the absence of TET, the MPF-mAb probe was intercepted by the TET-BSA on the *T*-line, exhibiting an obvious black line owing to the excellent optical properties of MPF. In the presence of TET, the MPF-mAb probe could conjugate the target TET, and the remaining MPF-mAb probe (which did not conjugate the target) was captured by the TET-BSA, showing a black line that was shallower than the negative test strip. When the concentration of the target was relatively high, it could completely combine with the MPF-mAb probe, and the *T*-line could not display visible color. Regardless of the TET concentration in the sample solution, the MPF-mAb probe migrated to the C-line and combined with the goat anti-mouse IgG due to the different binding sites. Therefore, the bright black band on the C-line would always be displayed. Since the clear colored MPF was captured at the *T*-line, the results could be easily monitored by the naked eye or recorded by a camera for quantitative determination (Fig. 1C).

3.2. Characterizations of the MPF and MPF-protein conjugation

As seen from Fig. 2A, scanning electron microscopic (SEM) image demonstrated that ZIF-67 had regular and smooth cubes of size about 200 nm, the average size of MPF was around 250 nm (Fig. 2C). Fig. 2B and D showed the transmission electron microscopy (TEM) element mapping of ZIF-67 and MPF, indicating homogeneous distributions of C_O, N, and O in them. Additionally, in the X-ray powder diffraction (XRD) patterns of MPF, the characteristic peak for ZIF-67 was absent (Fig. 2E), suggesting that ZIF-67 was successfully covered by PDA (Ren, Cai, Yu, Zeng, & Tang, 2018). Furthermore, the X-ray photoelectron spectroscopy (XPS) spectra (Fig. 2F) showed the peaks situated at approximately 797 eV and 781 eV, which could be attributed to Co $2p_{1/2}$ and Co $2p_{3/2}$ in the ZIF-67 and MPF, respectively. However, the two satellite peaks at 786 eV and 803 eV, assigned to the Co^{2+} oxidation state in ZIF-67, were absent in the spectrum of MPF, which further confirmed the successful preparation of MPF (Liang et al., 2017). The Fourier-transform infrared (FT-IR) spectrum was employed to analyze the functional groups of ZIF-67 and MPF. In Fig. 2G, the band at 425 cm^{-1} represented the C_O-N bond of ZIF-67, and the obtained peaks at 600–1500 cm^{-1} were ascribed to the stretching and bending modes of the imidazole ring. The band at 1584 cm^{-1} was caused by the stretching of C=N on 2-methylimidazole. The peak at 2930 cm^{-1} was caused by the C—H stretching mode of the aromatic ring and the fatty chain (Gross, Sherman, & Vajo, 2012; Lin & Chang, 2015; Qin et al., 2017). Moreover, three bands at 3200–3500 cm^{-1} and 1585 cm^{-1}

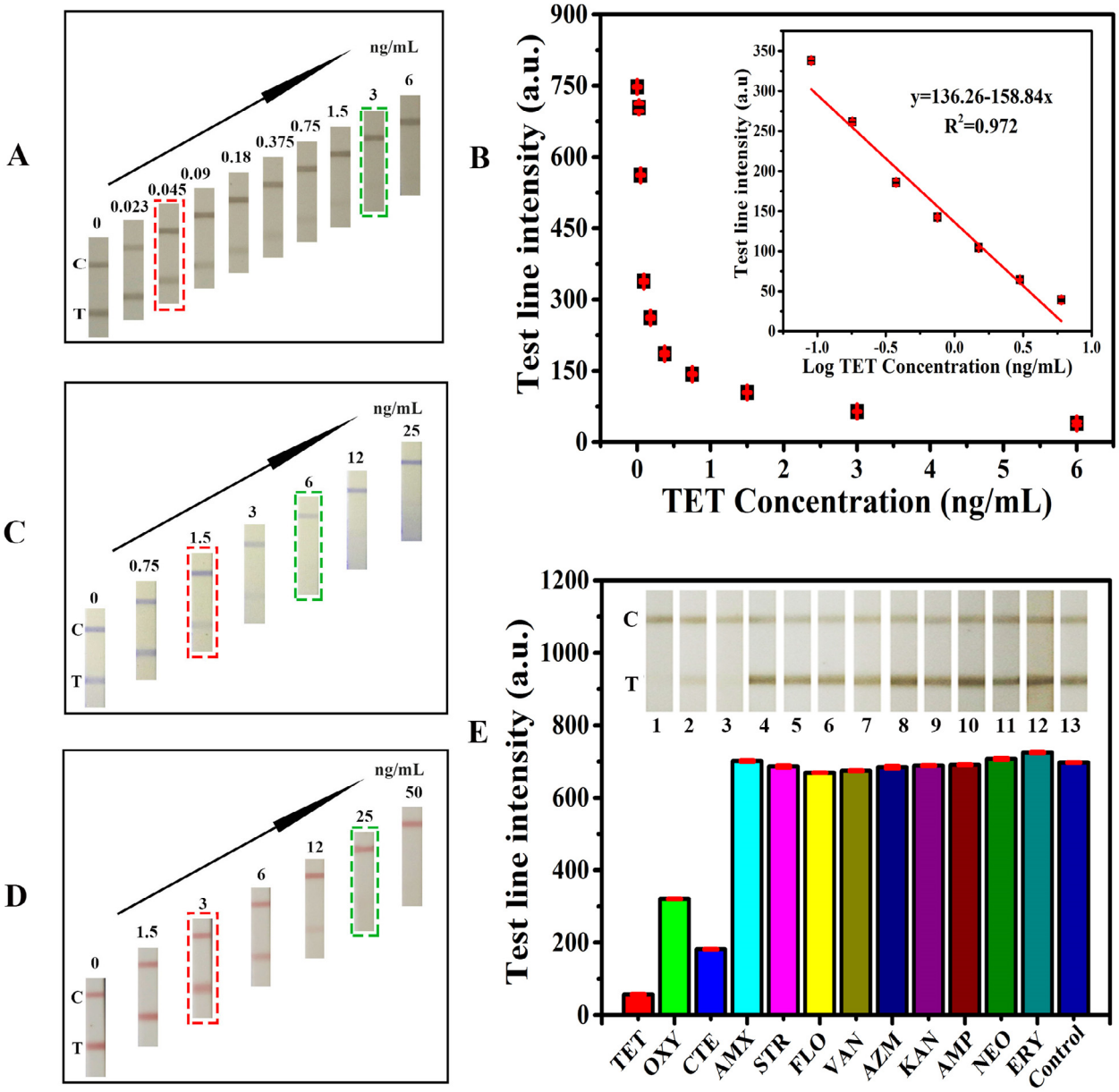

Fig. 4. (A) Sensitivity results of MPF-LFA for the detection of TET; (B) The variation rule of TET monitoring by the MPF-LFA in the whole detection concentration range (Inset image: Calibration curve of TET detection with concentration ranging from 0.09 to 6 ng/mL). Error bars indicate the standard errors of the three replicates. (C) Sensitivity results of ZIF-67-LFA for the detection of TET; (D) Sensitivity results of AuNP-LFA for the detection of TET; (E) Specificity of the assay to different antibiotics (Inset image: Nos. 1–13 correspond to TET, OXY, CTE, AMX, STR, FLO, VAN, AZM, KAN, AMP, NEO, ERY, and control, respectively).

were observed in the spectrum of MPF, which were related to the stretching vibrations of O—H/N—H and rang vibration of indole, respectively (Ren et al., 2018). All of these observations demonstrated the successful synthesis of ZIF-67 and MPF.

To further explore the conjugation ability of MPF, the band variation of MPF-mAb was measured using UV–visible spectroscopy. As can be seen from Fig. 2H, the pure MPF had no absorption peak. After binding to mAbs, a peak was observed at 280 nm, which corresponded to the characteristic peak of mAbs, indicating strong interactions between mAbs and MPF. In addition, for MPF, the labeling with mAbs changed the zeta potential from −3.68 mV to −0.22 mV, revealing that mAbs were loaded on the surface of MPF (Fig. 2I). Furthermore, BSA, MPF-BSA, and MPF were analyzed via sodium dodecyl sulfate polyacrylamide gel electrophoresis (SDS-PAGE). For BSA, a blue band appeared at a molecular weight of approximately 60 kDa (Putri, Handharyani, Soejoedono, Setiyono, & Poetri, 2018). When BSA was incubated with MPF, the band emerged at the same molecular weight as BSA (Fig. 2J). However, under the same conditions, pure MPF did not show the band, exhibiting that MPF successfully labeled BSA, indicating the label protein ability of MPF. The above results all testified the strong conjugation between MPF and protein.

In order to prove that MPF has an excellent stability, the stabilities of MPF, AuNPs, MPF-LFA and AuNP-LFA within 6 weeks were investigated. As shown in Fig. S1A and S1B, the *T*-line intensities of the MPF-LFA and AuNP-LFA all kept stable levels within 6 weeks. In addition, the MPF and AuNPs solutions still maintained splendid stability after storage at room temperature for 6 weeks (Fig. S1C and S1D), indicating the excellent stabilities of MPF and fabricated MPF-LFA. Moreover, the affinity for proteins between MPF and AuNPs were compared by determining the binding amount of BSA using a bicinchoninic acid (BCA) kit detection method. In Fig. S2, 25.61 μg of BSA was loaded on the MPF, while 10.98 μg of BSA was labeled on the AuNPs,

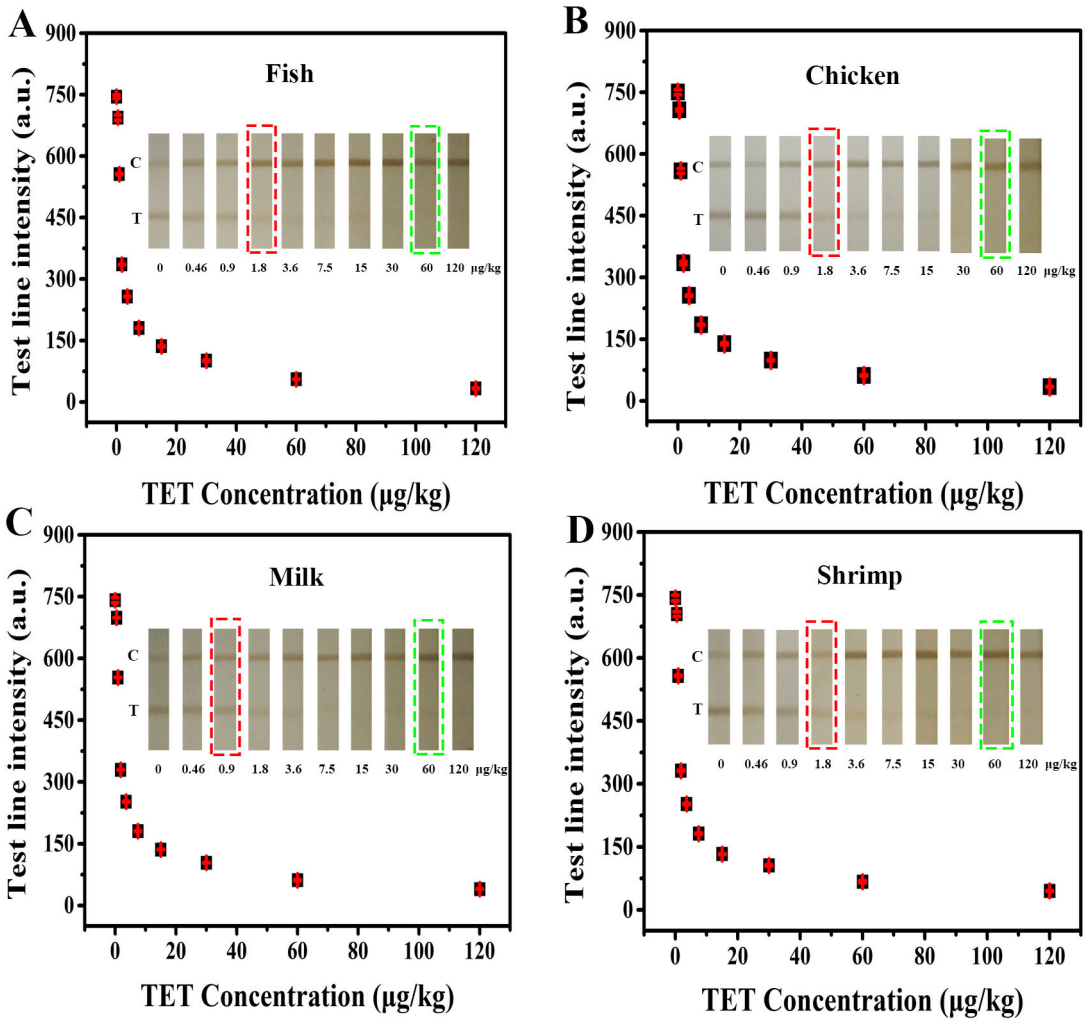

Fig. 5. Response of the MPF-LFA to TET with different concentrations in (A) fish, (B) chicken, (C) milk and (D) shrimp samples.

Table 1
Analytical results of TET spiked in food samples using the MPF-LFA and LC-MS (n = 3).

Sample	Spiked	Mean found ± SD (μg/kg)		Relative error (%) against LC-MS	Recovery (%) ± RSD[A] (%)	
	(μg/kg)	MPF-LFA	LC-MS		MPF-LFA	LC-MS
Fish	30	33.51 ± 0.82[a]	30.5 ± 0.5[a]	9.86	111 ± 2.4	101 ± 1.6
	60	63.12 ± 1.95[b]	57 ± 0.2[b]	10.73	105 ± 3.1	95 ± 0.4
Chicken	30	34.49 ± 0.62[a]	30.75 ± 1.25[a]	12.16	114 ± 1.8	102 ± 4.1
	60	58.99 ± 1.44[b]	58.88 ± 0.92[b]	0.19	98 ± 2.4	98 ± 1.5
Milk	30	32.11 ± 1.52[a]	29.9 ± 0.1[a]	7.39	107 ± 4.7	99 ± 0.4
	60	59.27 ± 1.06[b]	54.81 ± 0.99[b]	4.46	98 ± 1.8	91 ± 1.8
Shrimp	30	31.17 ± 0.76[a]	28.37 ± 0.73[a]	9.86	103 ± 2.4	94 ± 2.5
	60	54.62 ± 1.93[b]	56.19 ± 0.29[b]	−2.79	91 ± 3.6	93 ± 0.5

Different small letters in the same column indicate significant difference ($P \leq 0.05$).
[A] RSD, relative standard deviation.

indicating that MPF has a better affinity for proteins than traditional AuNPs.

3.3. Optimization of the experimental parameters

In order to guarantee the MPF-LFA has an excellent performance, we optimized the concentration of MPF, amount of mAbs, volume of the probe, and immunoreaction time. Firstly, we investigated the effect of MPF concentration (0.2–1.0 mg/mL). As illustrated in Fig. 3A, as the concentration of the MPF increased to 0.6 mg/mL, the *T*-line intensity strengthened gradually, and above 0.6 mg/mL, the *T*-line intensity decreased. Thus, 0.6 mg/mL was selected as the optimal concentration of MPF. The effect of the amount of mAbs was also surveyed in the range from 2 μg to 10 μg (Fig. 3B). The color of *T*-line deepened evidently with the increasing amount of mAbs, and maximal value of the *T*-line emerged at 8 μg, indicating that 8 μg was the optimum amount of anti-TET mAbs. It can be seen that when probe volume was 1.0 μL, the values of the two lines were closest, so, 1.0 μL of MPF-mAb probe was selected as optimal volume (Fig. 3C). As shown in Fig. 3D, as the immunoreaction time increased, the *T*-line intensity was increased and

reached a peak at 15 min, revealing that the reaction attained saturation. We further optimized the experimental parameters based on the ZIF-67-LFA and traditional AuNP-LFA (Fig. S3), the optimal amount of mAbs were 8 μg and 10 μg, respectively. The results indicated that the optimal amount of mAbs required for MPF was less than that of traditional AuNPs.

3.4. Analytical performance of the MPF-LFA

The sensitivity of the MPF-LFA for TET was investigated under the optimized conditions mentioned above (the detailed detection process is specified in Section 2.4). When the *T*-line was observed to be significantly faded compared to the negative test strip, the corresponding minimal TET concentration was defined as the visual limit of detection (vLOD). When the *T*-line completely disappeared, the corresponding minimal concentration was considered as the cut-off concentration. As can be seen from Fig. 4A and 4B, the *T*-line intensity dramatically decreased as the TET concentration increased, and the vLOD and cut-off value of the MPF-LFA for TET were 0.045 ng/mL and 3 ng/mL, respectively. Also, a good linear relationship of *T*-line intensity with the logarithm of TET concentration was seen in the range of 0.09–6 ng/mL with a relative coefficient (R^2) of 0.972 (inset in Fig. 4B).

In addition, ZIF-67-LFA and traditional AuNP-LFA were also used to detect the serial concentration of TET to value the improvement of MPF-LFA sensitivity. The vLOD and cut-off value of the ZIF-67-LFA for TET were 1.5 ng/mL and 6 ng/mL (Fig. 4C), respectively. Also, the vLOD and cut-off value of the AuNP-LFA for TET were 3 ng/mL and 25 ng/mL (Fig. 4D), respectively. In addition, comparison to the results of sensitivity for TET of other common detection methods (such as electrochemical immunosensing and near-infrared fluorescence-LFA, etc.), it could be proved that this MPF-LFA possessed high sensitivity (Table S1).

The specificity of the biosensor was determined by testing solutions containing both TET (6 ng/mL) and 11 other antibiotics. It is worth noting that the signal intensities on the *T*-line were inhibited to some extent since TET, OXY, and CTE belong to the class of isomers (Fig. 4E). Whereas the 9 other antibiotics exhibited a bright black color on the *T*-line, revealing excellent selectivity of the MPF-LFA sensor toward TET. In addition, selectivity was consistent with enzyme-linked immunosorbent assay (ELISA) (Fig. S4).

3.5. Application in actual samples

In this work, milk, shrimp, chicken, and fish were selected for spiked experiments to confirm the practicability of the sensor, and these matrices were previously tested to be free of TET by liquid chromatography-mass spectrometry (LC-MS) (Fig. S5). As shown in Fig. 5, the vLODs of TET in milk, shrimp, chicken and fish samples were 0.9, 1.8, 1.8 and 1.8 μg/kg, respectively, satisfying the limits permitted by the EU standard (100 μg/kg for TET) (Ge et al., 2018; Li et al., 2017). And when the concentrations of TET reached 60 μg/kg, no color could be monitored on *T*-line. Furthermore, the accuracy of the proposed MPF-LFA in real samples was evaluated by LC-MS methods. In Table 1, the recoveries of the MPF-LFA were ranging from 91% to 114% with relative standard deviation (RSD) values all below 4.7%, and the recoveries of the LC-MS were in the range of 91% to 102% with RSD values all below 4.1%. Moreover, the relative error against LC-MS was also below 12.16%. Thus, the results showed that developed sensor was well-suited for detecting TET in actual samples.

4. Conclusion

In summary, a highly sensitive biosensor using MPF as a label was designed for visual detection of TET. The assay displayed an admirable vLOD (0.045 ng/mL) with a detection range of 0.09 to 6 ng/mL. The MPF-LFA biosensor has obvious advantages compared with existing methods. Firstly, labeling MPF with mAbs via a simple mixing method, avoiding the complex cross-linking of mAbs. Furthermore, the MPF-based technology is cost-effective, a fewer mAbs were labeled on the MPF owning to the large specific surface area and excellent bioconjugation capacity of MPF compared with traditional AuNPs. Besides, the performance of MPF-LFA was comparable or better than other reported technologies. Most importantly, this biosensing platform was also successfully applied for detecting TET residues in milk, shrimp, fish, and chicken products. Thereby, it is anticipated that this work may opened a new window in structuring high-performance LFA for ultrasensitive and specific monitoring multitudinous small molecules.

CRediT authorship contribution statement

Yongming Tian: Conceptualization, Methodology, Formal analysis, Writing - original draft. **Tong Bu:** Conceptualization, Methodology, Formal analysis, Writing - original draft. **Meng Zhang:** Validation. **Xinyu Sun:** Investigation. **Pei Jia:** Resources. **Qinzhi Wang:** Resources. **Yingnan Liu:** Funding acquisition. **Feier Bai:** Funding acquisition. **Shuang Zhao:** Software. **Li Wang:** Conceptualization.

Declaration of Competing Interest

The authors declare that they have no known competing financial interests or personal relationships that could have appeared to influence the work reported in this paper.

Acknowledgments

This work was supported by Talented Program (A279021724) and the Fundamental Research Funds for the Northwest A&F University (Nos. Z111021601).

Appendix A. Supplementary data

Supplementary data to this article can be found online at https://doi.org/10.1016/j.foodchem.2020.127854.

References

Bragina, V. A., Znoyko, S. L., Orlov, A. V., Pushkarev, A. V., Nikitin, M. P., & Nikitin, P. I. (2019). Analytical platform with selectable assay parameters based on three functions of magnetic nanoparticles: Demonstration of highly sensitive rapid quantitation of *staphylococcal enterotoxin B* in Food. *Analytical Chemistry, 91*(15), 9852–9857. https://doi.org/10.1021/acs.analchem.9b01519.

Bu, T., Wang, J., Huang, L., Dou, L., Zhao, B., Li, T., & Zhang, D. (2019). New functional tracer—two-dimensional nanosheet-based immunochromatographic assay for *salmonella enteritidis* detection. *Journal of Agriculture and Food Chemistry, 67*(23), 6642–6649. https://doi.org/10.1021/acs.jafc.9b00374.

Chapman, R., Lin, Y., Burnapp, M., Bentham, A., Hillier, D., Zabron, A., ... Stevens, M. M. (2015). Multivalent nanoparticle networks enable point-of-care detection of human phospholipase-A_2 in serum. *ACS Nano, 9*(3), 2565–2573. https://doi.org/10.1021/nn5057595.

Chen, B., Yang, Z., Zhu, Y., & Xia, Y. (2014). Zeolitic imidazolate framework materials: Recent progress in synthesis and applications. *Journal of Materials Chemistry A, 2*(40), 16811–16831. https://doi.org/10.1039/c4ta02984d.

Chen, H., Qiu, Q., Sharif, S., Ying, S., Wang, Y., & Ying, Y. (2018). Solution-phase synthesis of platinum nanoparticle-decorated metal-organic framework hybrid nanomaterials as biomimetic nanoenzymes for biosensing applications. *ACS Applied Materials & Interfaces, 10*(28), 24108–24115. https://doi.org/10.1021/acsami.8b04737.

Chen, Y., Chen, Q., Han, M., Liu, J., Zhao, P., He, L., ... Zhang, L. (2016). Near-infrared fluorescence-based multiplex lateral flow immunoassay for the simultaneous detection of four antibiotic residue families in milk. *Biosensors & Bioelectronics, 79*, 430–434. https://doi.org/10.1016/j.bios.2015.12.062.

Dai, H., Chen, Y., Niu, X., Pan, C., Chen, H., & Chen, X. (2018). High-performance electrochemical biosensor for nonenzymatic H_2O_2 sensing based on Au@C-Co_3O_4 heterostructures. *Biosensors & Bioelectronics, 118*, 36–43. https://doi.org/10.1016/j.bios.2018.07.022.

El Alami El Hassani, N., Baraket, A., Boudjaoui, S., Taveira Tenorio Neto, E., Bausells, J., El Bari, N., & Zine, N. (2019). Development and application of a novel electrochemical immunosensor for tetracycline screening in honey using a fully integrated electrochemical Bio-MEMS. *Biosensors & Bioelectronics, 130*, 330–337. https://doi.

org/10.1016/j.bios.2018.09.052.
Ge, L., Li, H., Du, X., Zhu, M., Chen, W., Shi, T., ... Wang, K. (2018). Facile one-pot synthesis of visible light-responsive $BiPO_4$/nitrogen doped graphene hydrogel for fabricating label-free photoelectrochemical tetracycline aptasensor. *Biosensors & Bioelectronics, 111*, 131–137. https://doi.org/10.1016/j.bios.2018.04.008.
Gomez-Martinez, J., Silvy, M., Chiaroni, J., Fournier-Wirth, C., Roubinet, F., Bailly, P., & Bres, J. C. (2018). Multiplex lateral flow assay for rapid visual blood group genotyping. *Analytical Chemistry, 90*(12), 7502–7509. https://doi.org/10.1021/acs.analchem.8b01078.
Gross, A. F., Sherman, E., & Vajo, J. J. (2012). Aqueous room temperature synthesis of cobalt and zinc sodalite zeolitic imidizolate frameworks. *Dalton Transactions, 41*(18), 5458–5460. https://doi.org/10.1039/c2dt30174a.
Hu, H., Guan, B. Y., & Lou, X. W. (2016). Construction of complex CoS hollow structures with enhanced electrochemical properties for hybrid supercapacitors. *Chem, 1*(1), 102–113. https://doi.org/10.1016/j.chempr.2016.06.001.
Hu, J., Jiang, Y. Z., Wu, L. L., Wu, Z., Bi, Y., Wong, G., ... Zhang, Z. L. (2017). Dual-signal readout nanospheres for rapid point-of-care detection of *ebola virus* glycoprotein. *Analytical Chemistry, 89*(24), 13105–13111. https://doi.org/10.1021/acs.analchem.7b02222.
Kim, J., Kwon, J. H., Jang, J., Lee, H., Kim, S., Hahn, Y. K., & Lee, J. (2018). Rapid and background-free detection of avian influenza virus in opaque sample using NIR-to-NIR upconversion nanoparticle-based lateral flow immunoassay platform. *Biosensors & Bioelectronics, 112*, 209–215. https://doi.org/10.1016/j.bios.2018.04.047.
Kreno, L. E., Leong, K., Farha, O. K., Allendorf, M., Van Duyne, R. P., & Hupp, J. T. (2011). Metal–organic framework materials as chemical sensors. *Chemical Reviews, 112*(2), 1105–1125. https://doi.org/10.1021/cr200324t.
Li, C., Zhu, L., Yang, W., He, X., Zhao, S., Zhang, X., ... Li, Z. (2019). Amino-functionalized Al-MOF for fluorescent detection of tetracyclines in milk. *Journal of Agriculture and Food Chemistry, 67*(4), 1277–1283. https://doi.org/10.1021/acs.jafc.8b06253.
Li, H., Li, J., Qiao, Y., Fang, H., Fan, D., & Wang, W. (2017). Nano-gold plasmon coupled with dual-function quercetin for enhanced photoelectrochemical aptasensor of tetracycline. *Sensors and Actuators B: Chemical, 243*, 1027–1033. https://doi.org/10.1016/j.snb.2016.12.032.
Liang, Y., Wei, J., Hu, Y. X., Chen, X. F., Zhang, J., Zhang, X. Y., ... Wang, H. T. (2017). Metal-polydopamine frameworks and their transformation to hollow metal/N-doped carbon particles. *Nanoscale, 9*(16), 5323–5328. https://doi.org/10.1039/c7nr00978j.
Lin, K. Y. A., & Chang, H. A. (2015). Zeolitic imidazole framework-67 (ZIF-67) as a heterogeneous catalyst to activate peroxymonosulfate for degradation of rhodamine B in water. *Journal of the Taiwan Institute of Chemical Engineers, 53*, 40–45. https://doi.org/10.1016/j.jtice.2015.02.027.
Mehta, J., Dhaka, S., Bhardwaj, N., Paul, A. K., Dayananda, S., Lee, S. E., ... Deep, A. (2019). Application of an enzyme encapsulated metal-organic framework composite for convenient sensing and degradation of methyl parathion. *Sensors and Actuators B: Chemical, 290*, 267–274. https://doi.org/10.1016/j.snb.2019.03.116.
Putri, D. D., Handharyani, E., Soejoedono, R. D., Setiyono, A., & Poetri, O. N. (2018). Production and characterization of newcastle disease antibody as a reagent to develop a rapid immunodiagnostic test tool. *Veterinary World, 11*(7), 895–901. https://doi.org/10.14202/vetworld.2018.895-901.
Qin, J., Wang, S., & Wang, X. (2017). Visible-light reduction CO_2 with dodecahedral zeolitic imidazolate framework ZIF-67 as an efficient co-catalyst. *Applied Catalysis, B: Environmental, 209*, 476–482. https://doi.org/10.1016/j.apcatb.2017.03.018.
Qiu, Q., Chen, H., Sharif, S., You, Z., Ying, S., Wang, Y., & Ying, Y. (2019). Ultrathin noble metal nanoplates decorated metal-organic framework nanosheets as 2D/2D heterojunction nanobionic catalysts for explosive residues monitoring. *2D Materials, 6*(3), Article 035008. https://doi.org/10.1088/2053-1583/ab1165.
Qiu, Q., Chen, H., Ying, S., Sharif, S., You, Z., Wang, Y., & Ying, Y. (2019). Simultaneous fluorometric determination of the DNAs of *salmonella enterica*, *listeria monocytogenes* and *vibrio parahemolyticus* by using an ultrathin metal-organic framework (type Cu-TCPP). *Mikrochimica Acta, 186*(2), 93. https://doi.org/10.1007/s00604-019-3226-y.
Qiu, Q., Chen, H., You, Z., Feng, Y., Wang, X., Wang, Y., & Ying, Y. (2020). Shear exfoliated metal-organic framework nanosheet-enabled flexible sensor for real-time monitoring of superoxide anion. *ACS Applied Materials & Interfaces, 12*(5), 5429–5436. https://doi.org/10.1021/acsami.9b17659.
Ren, R., Cai, G., Yu, Z., Zeng, Y., & Tang, D. (2018). Metal-polydopamine framework: An innovative signal-generation tag for colorimetric immunoassay. *Analytical Chemistry, 90*(18), 11099–11105. https://doi.org/10.1021/acs.analchem.8b03538.
Sheng, W., Chang, Q., Shi, Y., Duan, W., Zhang, Y., & Wang, S. (2018). Visual and fluorometric lateral flow immunoassay combined with a dual-functional test mode for rapid determination of tetracycline antibiotics. *Mikrochimica Acta, 185*(9), 404. https://doi.org/10.1007/s00604-018-2945-9.
Sumida, K., Rogow, D. L., Mason, J. A., McDonald, T. M., Bloch, E. D., Herm, Z. R., ... Long, J. R. (2012). Carbon dioxide capture in metal-organic frameworks. *Chemical Reviews, 112*(2), 724–781. https://doi.org/10.1021/cr2003272.
Taranova, N. A., Berlina, A. N., Zherdev, A. V., & Dzantiev, B. B. (2015). 'Traffic light' immunochromatographic test based on multicolor quantum dots for the simultaneous detection of several antibiotics in milk. *Biosensors & Bioelectronics, 63*, 255–261. https://doi.org/10.1016/j.bios.2014.07.049.
Wang, J., Cheng, R., Wang, Y., Sun, L., Chen, L., Dai, X., ... Yan, Y. (2018). Surface-imprinted fluorescence microspheres as ultrasensitive sensor for rapid and effective detection of tetracycline in real biological samples. *Sensors and Actuators B: Chemical, 263*, 533–542. https://doi.org/10.1016/j.snb.2018.02.150.
Wang, T., Mei, Q., Tao, Z., Wu, H., Zhao, M., Wang, S., & Liu, Y. (2020). A smartphone-integrated ratiometric fluorescence sensing platform for visual and quantitative point-of-care testing of tetracycline. *Biosensors & Bioelectronics, 148*, Article 111791. https://doi.org/10.1016/j.bios.2019.111791.
Wang, Y., Yao, L., Ning, G., Wu, Y., Wu, S., Mao, S., & Liu, G. Q. (2019). An electrochemical strategy for tetracycline detection coupled triple helix aptamer probe with catalyzed hairpin assembly signal amplification. *Biosensors & Bioelectronics, 143*, Article 111613. https://doi.org/10.1016/j.bios.2019.111613.
Xu, X., Ji, D., Zhang, Y., Gao, X., Xu, P., Li, X., ... Wen, W. (2019). Detection of phenylketonuria markers using a ZIF-67 encapsulated PtPd alloy nanoparticle (PtPd@ZIF-67)-based disposable electrochemical microsensor. *ACS Applied Materials & Interfaces, 11*(23), 20734–20742. https://doi.org/10.1021/acsami.9b05431.
Yan, P., Jiang, D., Tian, Y., Xu, L., Qian, J., Li, H., ... Li, H. (2018). A sensitive signal-on photoelectrochemical sensor for tetracycline determination using visible-light-driven flower-like CN/BiOBr composites. *Biosensors & Bioelectronics, 111*, 74–81. https://doi.org/10.1016/j.bios.2018.03.054.
Zhang, D., Li, P., Zhang, Q., & Zhang, W. (2011). Ultrasensitive nanogold probe-based immunochromatographic assay for simultaneous detection of total aflatoxins in peanuts. *Biosensors & Bioelectronics, 26*(6), 2877–2882. https://doi.org/10.1016/j.bios.2010.11.031.
Zhang, L., & Chen, L. (2016). Fluorescence probe based on hybrid mesoporous silica/quantum dot/molecularly imprinted polymer for detection of tetracycline. *ACS Applied Materials & Interfaces, 8*(25), 16248–16256. https://doi.org/10.1021/acsami.6b04381.
Zhao, P., Wu, Y., Zhu, Y., Yang, X., Jiang, X., Xiao, J., ... Li, C. (2014). Upconversion fluorescent strip sensor for rapid determination of *vibrio anguillarum*. *Nanoscale, 6*(7), 3804–3809. https://doi.org/10.1039/c3nr06549a.